Solid State Electrolyte Gate Transistor with Ion Doping for Bio-signal Classification of Neuromorphic Computing.

Qinan Wang, Tianshi Zhao, Chun Zhao, Wen Liu*, Li Yang, Yina Liu*, Dian Sheng, Rongxuan Xu, Yutong Ge, Xin Tu, Hao Gao, Cezhou Zhao*

Q. Wang, T. Zhao, Prof. C. Zhao, Prof. W. Liu, D. Sheng, R. Xu, Y. Ge
School of Advanced Technology, Xi'an Jiaotong-Liverpool University, Suzhou 215123, China
E-mail: Chun.Zhao@xjtlu.edu.cn; Wen.Liu@xjtlu.edu.cn

Dr. Y. Liu
Department of Applied Mathematics, Xi'an Jiaotong-Liverpool University, Suzhou 215123, China
E-mail: Yina.Liu@xjtlu.edu.cn

Q. Wang, T. Zhao, D. Sheng, R. Xu, Y. Ge, Prof. X. Tu, Prof. C. Zhao
Department of Electrical Engineering and Electronics, University of Liverpool, Liverpool L69 3GJ, U.K.

L. Yang
Department of Chemistry, Xi'an Jiaotong-Liverpool University, Suzhou 215123, China

H. Gao
Department of Electrical Engineering, Eindhoven University of Technology, Den Dolech 2, 5612 AZ, The Netherlands

Keywords: synaptic transistor, neuromorphic computing, recognition of image and ECG, in-memory computing

Abstract text. As the core component of an intelligent neuromorphic computer system, reliable synaptic devices process vast amounts of data with high computing speed and low energy consumption. In this work, we propose the ion-doped eco-friendly solution-processed indium oxide (InO_x)/aluminum oxide (AlO_x) electrolyte gate transistors (EGTs) with typical and reliable synaptic behavior. The lithium (Li) ions doped into the AlO_x solid state layer to

facilitate the generation of electrical double layers (EDLs) and doped into InO_x to improve the stability of long-term potentiation/depression (LTP/LTD) cyclic update and enhance the synaptic plasticity. Finally, an artificial neural network (ANN) simulator is well designed to electrocardiogram (ECG) signal recognition based on the G_{max}/G_{min} ratio and nonlinearity of weight update curve. According to the results, the device possesses tremendous potential for bio-signal prediction and neural intervention. Moreover, for the first time, the recognition accuracy of the abnormality of the cardiovascular can reach over the 94.8% obtained from the confusion matrix. Consequently, this research article presents a stable and robust neuromorphic device for bio-signal recognition based on solid state EGTs via the synaptic long-term plasticity.

1. Introduction

The advanced computing system with a bionic nervous neuromorphic structure to facilitate parallel data updates for artificial neural networks (ANNs) has aroused extensive concern due to the limitations of conventional logic operation rules based on the von Neumann architecture.[1, 2] In order to construct the core units for the ANN system, the artificial synaptic transistors were then proposed for multi-level storage and parallel computing, which has been being intensively investigated to mimic the behavior and function of the biological synapses.[3, 4] According to the various storage mechanisms and physics, the ferroelectric transistors,[5-7] floating-gate transistors,[8,9] electrolyte gate transistors,[10,11] and electret-based organic transistors have been researched to realize the neurons behaviors.[12] Nevertheless, neuromorphic device , synaptic long-term plasticity and mechanisms of bionic synapse must be further explored to simultaneously enable signal transmission, iterative learning, and timely surveillance.[13]

The synaptic electrolyte gate transistors (EGTs) with transparent metal oxide as the dielectric layers and semiconductor layers possess the potential to obtain multi-level storage and cyclic update.[14] The gate dielectrics manufactured by general mechanism are not considered to be adequate for the requirements of a large retention range for memory and learning due to the lack of large hysteresis observed from the transfer characteristics curve.[15,16] Inspired by the biological nerve, ion doping can effectively solve this bottleneck which is also the mechanism of EGT. Compared with the bionic neural network produced by current CMOS process based on the von Neumann architecture, the synaptic devices have efficient parallel processing speed and low energy consumption for complex tasks.[17,18] The EGT makes it possible to achieve synaptic plasticity, weight updating and bionic neural

networks with small-scale and lower energy consumption per spike. The ions in the electrolyte layer of EGTs are regulated to migrate under the electric field effect and adjust the channel conductance.[19, 20] According to the migration extent of ions in the electrolyte layer, the working modes of adjusting the conductance could be divided into electrostatics modulation mode and electrochemical modulation mode.[19, 20, 21] According to previous studies, the Li^+ ion has been proved to facilitate the formation of electrical double layer (EDL) easily belongs to electrostatics mode due to the small ion radius and high diffusion coefficient.[22] In addition, Li^+ ion doping in the semiconductor could effectively reduce the oxygen vacancy, which significantly benefits the stability of the device.[23] Compare with the organic materials and 2-dimensional material as the partial structure of synaptic transistors, the solution-processed metal oxide materials have the advantage of large-scale preparation, simple fabrication and stability in environmental change.[24,25] However, recently, few studies have focused on the influence of Li^+ doping in the dielectric and semiconductor layers of EGTs for neural computation.

In this work, solid state electrolyte gate transistor with Li^+ ions doping has been proposed for neuromorphic computing. The Li^+ ions doping into AlO_x (dielectric layer) to enhance the synaptic long-term plasticity and charge storage ability. Purpose of Li^+ doping into the InO_x (semiconductor) layer for improving the stability apparently due to the cyclic update (cycle-to-cycle error). The doping concentration in the AlO_x and InO_x layers have been well discussed systematically. The typical synaptic behaviors, including inhibitory/excitatory postsynaptic current (IPSC/EPSC), long-term potentiation/depression (LTP/LTD), short-term potentiation (STP), and paired-pulse facilitation (PPF), have been successfully illuminated through the voltage spikes applied to the presynaptic terminal. It is worth noting that both the EPSC and IPSC are induced by the increase and decrease of channel conductance, respectively, which could be regarded as the change of synaptic weight. According to the G_{max}/G_{min} ratio and nonlinearity trend curves of LTP/LTD curve, the iterative update of synaptic weight matrix is demonstrated with the increase of epoch and the recognition accuracy of the bio-signal (ECG) can reach over the 94.8%.[26] Moreover, the neural network can predict the abnormal beats of the cardiovascular due to extreme weight regions. We believe that this systematic research of Li^+ ion-doped solid state EGTs would pave the way for future neuromorphic computing networks.

2. Results and Discussion

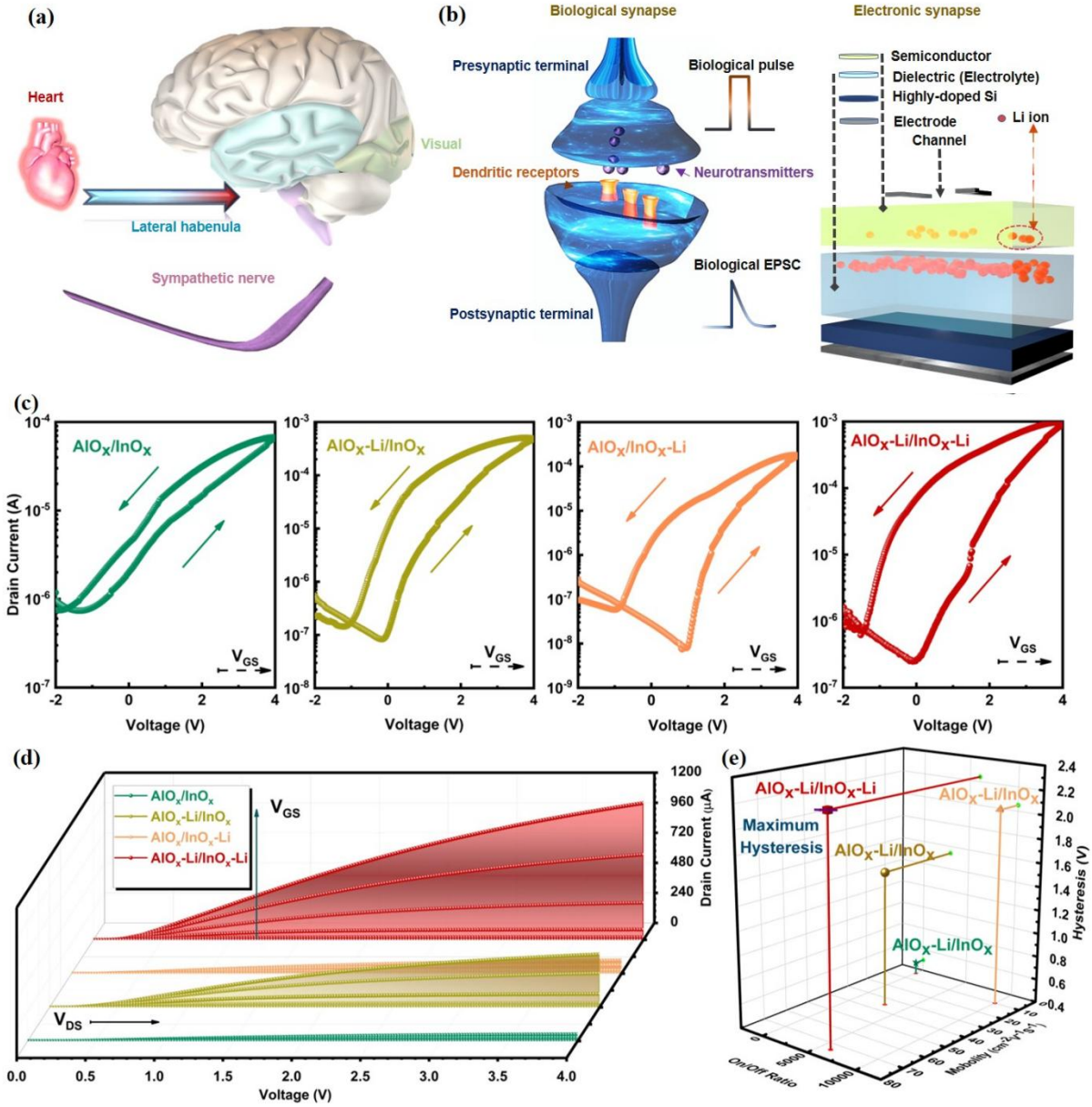

Figure 1. (a) Schematic diagram of the cranial nerve stimulated by light and ECG signals. (b) Schematics illustration of the biological synapse and the solution-processed synaptic EGTs. (c) Transfer characteristics of four different doping EGTs (AlO_x/InO_x AlO_x-Li/InO_x, AlO_x/InO_x-Li, and AlO_x-Li/InO_x-Li). (d) Output characteristic curves of the four different types EGTs. (e) Parameters (on/off current ratio, mobility, and hysteresis) of EGTs extracted from the transfer characteristics curves.

The brain directly recognizes signals from visual receptors, but lateral habenula (LHb) indirectly controls the cardiovascular by stimulating the sympathetic nerve (**Figure 1**a).[27] Compared with visual recognition, this phenomenon shows the importance of abnormal ECG recognition. All these functions depend on the biological synapses, which are the fundamental

components of information recollection, understanding, and computation modules.[28] Synapse is a juncture that conveys biological impulses between the presynaptic and postsynaptic terminals (Figure 1b, left).[5] Typically, neurotransmitters in the synaptic vesicle, which carry the biological and chemical information, travel through the synapse to enter the dendritic receptor. This mechanism transforms the chemical signal into an electrical pulse, eventually producing an EPSC.[29] Structural and functional resemblances between a biological synapse and a solution-processed artificial synapse are reflected about the gate electrode can be regarded as a presynaptic terminal and the drain electrode as a postsynaptic terminal (Figure1b, right). The electronic solution-processed synaptic transistors generate artificial EPSC and realize diverse synaptic plasticity based on the gate voltage applied to the n^+ Si bottom electrode activates a similar presynaptic pulse signal. The spin coated AlO_x and InO_x layers have the advantage of high k material, stability in the air and less defect states. The thin films were fabricated on heavily doped n^+-Si substrates by alumina (AlO_x), Li^+ ion-doped doped alumina (AlO_x-Li), indium oxide (InO_x), and Li^+ ion-doped doped indium oxide (InO_x-Li) precursor solutions. The AlO_x and AlO_x-Li layers (dielectric) were both annealed at 200°C, the InO_x and InO_x-Li layers (semiconductor) were both annealed at 300°C. The chemical compositions of Li-ion doping synaptic EGTs are verified by X-ray photoelectron spectroscopy (**Figure S1**). The normalized Li 1s spectra of four type EGTs are obtained by standard the C 1s peak. In order to compare the n-type transistor characteristic parameters of the synaptic EGTs with four doping types, the transfer curves of the system with V_{GS} (gate voltage) sweeping at a rate of 20 mV s^{-1} were evaluated and plotted (Figure 1c). The AlO_x-Li/InO_x-Li EGT demonstrate a clear counterclockwise hysteresis and a large change ratio of 2630 at V_g=0 due to the Li^+ ions migration. Different Li^+ ions doping concentration in AlO_x thin film would determine the formation strengths of electrostatic and electrochemical modulations. The synaptic plasticity of STP/LTP at different doping concentrations is analyzed and compared by applying incremental electric pulse to the gate. The appropriate doping concentration in AlO_x films is 10% according to the preferred performance of LTP that the large range of conductance from STP to LTP. (**Figure S2**). The doping concentration in the InO_x layer is based on the stability of the cyclic test. The on/off current ratios are 100, 8000, 10000, and 6000, respectively belonging to AlO_x/InO_x, AlO_x/InO_x-Li, AlO_x/InO_x-Li, and AlO_x-Li/InO_x-Li EGTs. The migration of Li^+ within the AlO_x and InO_x layers contributes to the hysteresis behavior, which can be observed through the transfer characteristic curves of four synaptic EGTs. The large hysteresis indicates channel conductance changes, which is a significant synaptic characteristic in the EGTs for neural network simulation.[20] Hysteresis

phenomenon is not only because of ion migration and ion pass through the interface between dielectric and channel but also due to oxygen vacancy from the low-temperature technology. In addition, the relatively smooth film surface can improve the yield and synaptic plasticity of the EGTs. Significantly, the smooth and uniform dielectric (AlO_x and AlO_x-Li) and semiconductor (InO_x and InO_x-Li) thin films are obtained by AFM deflection images (**Figure S3**). The root mean square (RMS) roughness of AlO_x, AlO_x-Li, InO_x, and InO_x-Li thin films are 1.552, 2.084, 0.380 and 0.306 nm, respectively. A simulated parallel neural computing system requires high plasticity and stability of the synaptic EGTs to update synaptic weights accordingly. Similarly, the SEM image clearly demonstrates the synaptic device structure for the AlOx (30 nm)/InOx (15 nm) and the parameters about the channel are W=150 μm and L=10 μm (**Figure S4**). The output curves indicate the apparent pinch-off voltage and saturation current indicating good ohmic contact between Al electrodes and the InO_x or InO_x-Li channel layer (Figure 1d). Three-dimensional graphic displays the comparison of three parameters (on/off current ratio, mobility, and hysteresis) between four types of synaptic EGTs (Figure 1e). It could be clearly observed that all the Li^+ doped EGTs, including AlO_x-Li/InO_x, AlO_x/InO_x-Li, and AlO_x-Li/InO_x-Li, exhibit more symmetrical hysteresis window than the AlO_x/InO_x device, which complies with the principle of ion migration.

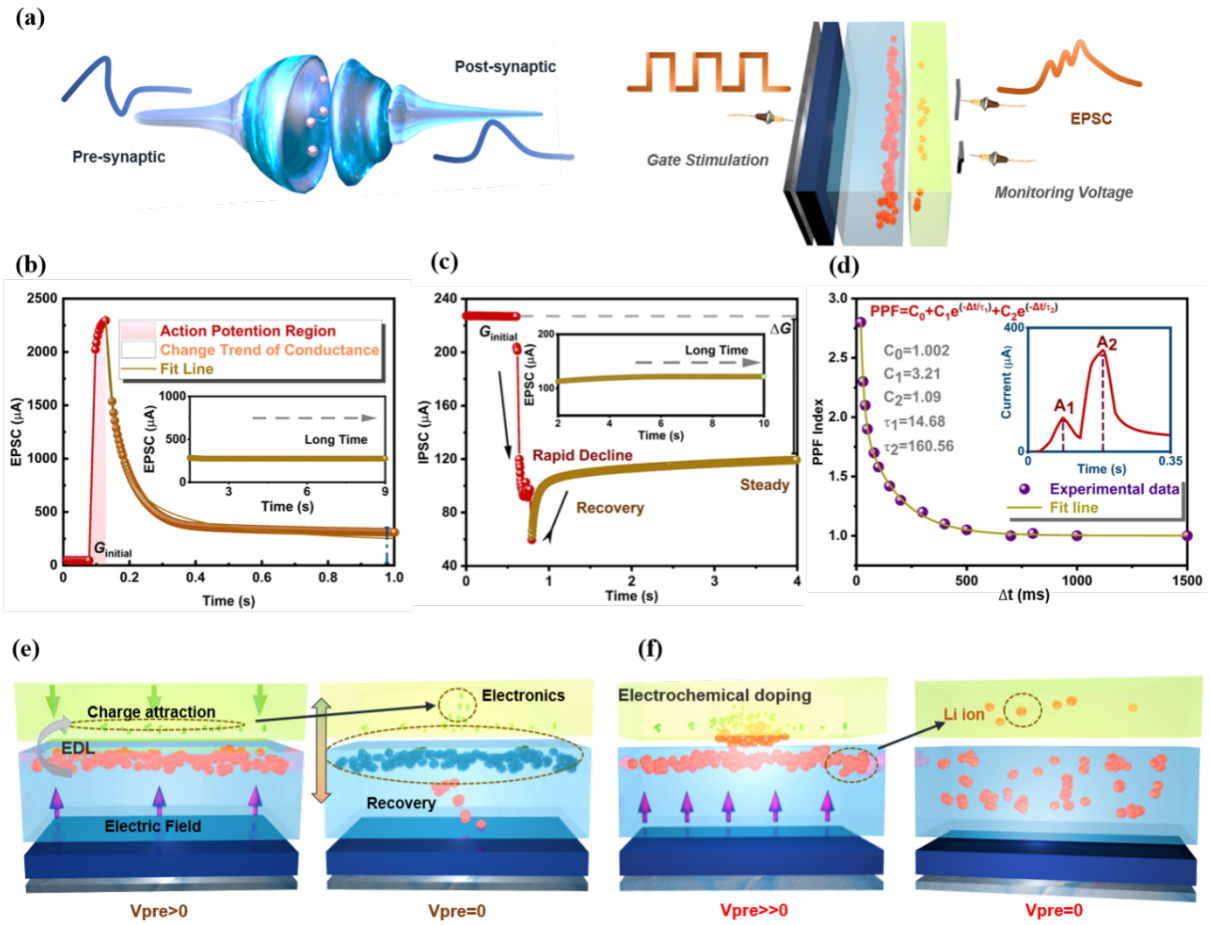

Figure 2. (a) Schematic illustration of signal transmission in biological synapse and electrical evaluation for artificial synaptic plasticity. (b) EPSC property triggered by presynaptic spikes (6 V 50 ms) in 1 s. (c) IPSC property triggered by presynaptic pulses (-6 V 50 ms) in 4s. (d) PPF index versus interval time Δt between two negative pulses (5 V). Inset: definitions of A_2 and A_1 with two successional 60 ms pulses. (e) Li^+ ion migration in the dielectric layer under weak gate bias stimuli for short-term potentiation. (f) Li^+ ion migration in the dielectric layer under strong gate bias stimuli for long-term potentiation.

The information transmission between presynaptic and postsynaptic terminals can be simulated by applying an electrical pulse to the gate and a monitoring voltage to the drain (**Figure 2**a). EPSC and IPSC are the elemental information flow, processing processes, and synaptic plasticity for a neuron to carry out intricate computing and retain synaptic weight.[30] In order to indicate the synaptic behaviors acquired from the typical EPSC and IPSC curves, the two numerical equivalent positive (6 V, 50 ms) and negative (-6 V, 50 ms) voltage spikes were applied to the gate terminal (Figure 2b, c). The insert figures of EPSC/IPSC show long-term potentiation for the longer period. The EPSC increased rapidly from the initial value to 2.4 mA after electrical stimulation, which is shown in the active region, and then decreased

slowly from peak value to 310 μA in 1 s. The drain current (PSC) stays steady as a result of no change in conductance prior to the operation of the pre-terminal voltage pulse. When a voltage pulse is applied to the gate of a synaptic transistor, lithium ions will migrate from AlO_x to the channel, resulting in an improvement in channel current and the formation of EPSC.[14] When the pulse stimulation ends, the ions near the channel electrolyte interface will diffuse away from the interface due to the Li^+ concentration gradient. Thereafter, the downward trend in the channel contributes to the inhibition of PSC when the presynaptic impulses are negative, thus generating an inhibitory postsynaptic current (IPSC).[31,32] The IPSC includes the rapid decline region, recovery area, and conductance stability section. The current after negative voltage stimulation changes from initial value 230 μA to steady 118 uA since Li^+ ions are considered to cross from the InO_x layer to the AlO_x layer. Further, to verify the low energy consumption of synaptic EGT, the energy consumption per spike of EGT is calculated by the Equation $E= I_{peak} \times t \times V$ =22.79 nJ (**Figure S5**). I_{peak} is the maximum value (455.8 nA) of generated EPSC, t is the spike duration (500 ms), and V is the voltage applied to the drain electrode (0.1 V).

Change of the conductance illustrates that the accelerated concentration of electrons/holes enhancement or suppression in the channel results from broad positive or negative voltage, resulting in a comparatively large (EPSC) and low (IPSC) conductivity than the original ones until the pulse is withdrawn. The change of channel conductance is simultaneously triggered by the pulse voltage modulation of the gate. This partly originated by the oxygen vacancy in the dielectric layer. Under the action of the electric field, oxygen vacancies act as traps to attract electrons or holes into the AlO_x or AlO_x-Li layer. Interestingly, presynaptic neurons regulate EPSC/IPSC through neurotransmitter transduction, while gate electrodes control channel conductance through the transfer of the charge carrier.[23]

In order to explain the phenomenon of conductance change in the dielectric layer due to Li^+ migration in detail, the schematic diagram of the movement of ions by voltage stimulation is proposed (Figure 2e, f). Via two modules of ion electronic modulation processes, these Li^+ ions accumulate, and electrons are attracted near the dielectric layer/channel interface: electronic double layer modulation (under weak electric field in Figure 2e) and electrochemical doping (under enhanced electric field in Figure2f). When the programmed V-pre is added to the EGTs presynaptic terminal, the limited radius and larger diffusion coefficient Li^+ ions effortlessly drift towards and cross the dielectric layer/channel interface due to the field accelerated ion migration.[19] With the weak spike stimulation (0-3 V), Li^+ ions shift under the electric field and accumulate at the interface and attract electrons, resulting in

short-term potential. With the enhanced spike stimulation (4-6 V), Li^+ ions across the AlO_x-Li/InO_x-Li interface, subsequently led to the formation of electrochemical doping. Li^+ ions and electronics gradually diffuse back to the original state of equilibrium with uniform composition when V_{pre} = 0 in both situations (weak and robust stimulation). According to the above mechanism, the hysteresis phenomenon in the transfer characteristic curve of EGT can be explained clearly. When a positive voltage applied to the gate from -2 to 4 V, the Li ions in the electrode migrate to the interface (form the EDL) and then intercalated into the channel with increasing the voltage amplitude (electrochemical doping). Then the positive reduced from the 4 V, the Li^+ ions accumulated in the interface recover into the dielectric layer (electrolyte) due to the concentration gradient of ions (internal field). With the negative voltage decrease to the -2 V, the ions migrate back to the electrode and the conductance restore the initial state. Moreover, we evaluate the synaptic plasticity of different dielectric layer thicknesses to verify the parameters of device influence the synaptic transistor according to the mechanism of synaptic EGTs (**Figure S6**). Paired pulse facilitation (PPF) is another universal form of short-term synaptic plasticity, which is the fundamental type of STP, also the linchpin to processing sound and temporal image information in the neuron (Figure 2d). Two stationary amplitude and width pulses (5 V, 60 ms) are applied to the presynaptic terminal with the interval of 2 s, and the postsynaptic current is evaluated with source-drain voltage (V_{DS}) of 1 V. EPSC will continue to decay after the end of the first pulse (A_1) stimulation before the arrival of the second stimulation until the Li^+ ions in the electrolyte return to the equilibrium position.[23] If the second stimulus (A_2) is triggered before the whole remaining Li^+ ions are recovered, the remaining Li^+ ions will be superimposed by the second stimulus, furthermore, increase the amplitude of EPSC. The following expression can be described and evaluated as the PPF index.

$$\mathrm{PPF} = \frac{A_2}{A^1} * 100\% \quad (1)$$

Under the minimum time interval, the double-pulse facilitation coefficient((A_2/A_1) is the maximum. The following function expresses the relation between PPF and Δt.

$$\mathrm{PPF} = C_0 + C_1\, e^{\left(-\frac{\Delta t}{\tau 1}\right)} + C_2\, e^{\left(-\frac{\Delta t}{\tau 2}\right)} \quad (2)$$

Initial constants of rapid and slow phases C_0, C_1, and C_2 are 1, 23%, and 45%. The relaxation times are $\tau 1$(20 ms) and $\tau 2$(65 ms).

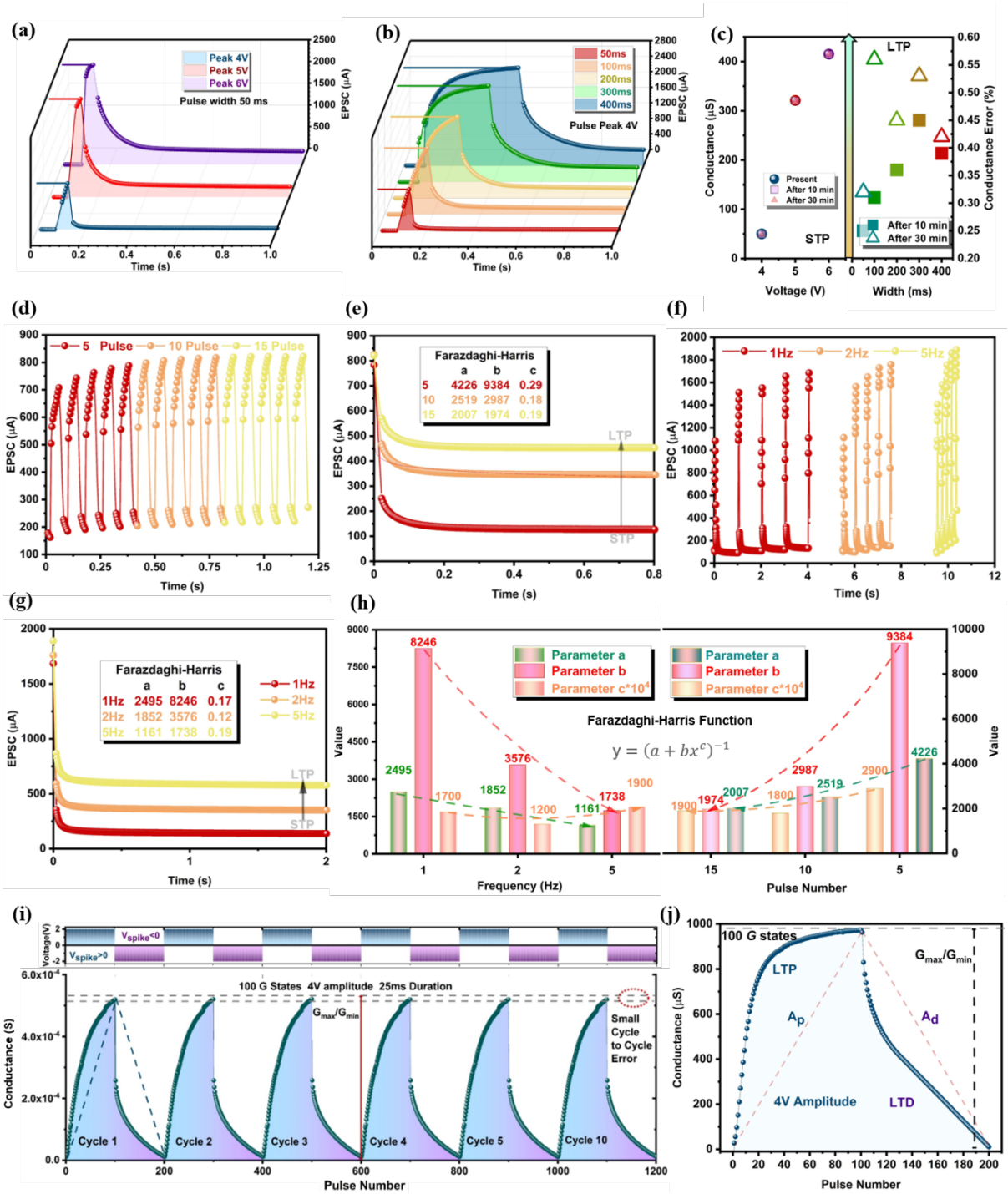

Figure 3. (a) EPSC triggered by three pulses with different amplitudes (4, 5, and 6 V) at V_{DS} = 4 V. (b) EPSC triggered by five pulses with different durations (50, 100, 200, 300, and 400 ms) at V_{DS}=4 V. (c) Stable conductance multi-level from STP to LTP for different voltages and widths. (d) EPSC stimulated by a sequence of 15 voltage pulses (5, 10, and 15 pulses) with the 50 ms period and 4 V amplitude. (e) STP to LTP conversion process in 0.8 s under 5, 10, and 15 presynaptic pulses. (f) EPSC stimulated by five continuous pulses (4 V, 40 ms) with different frequencies (1, 2, and 5 Hz). (g) Process of STP to LTP conversion in 2 s with different frequencies. (h) Fitting of the attenuation process to the curve of Farazdaghi-Harris

function showing a trend of the three parameters (a, b, c). (i) Increasing and decreasing of channel conductance illustrating the long-term potentiation and long-term depression (LTP/LTD) characteristics triggered by 100 positive (5V, 50 ms) and 100 negatives (-4 V, 50 ms) continuous spike signals. (j) Channel conductance modulation of weight update for 10 repeated 100 positive pulses (4 V Δt = 50 ms) and 40 negative pulses (-4 V Δt = 50 ms).

To simulate the synaptic memory-guided behavior inspired from short-term memory (STM) and long-term memory (LTM) in the human brain, the EGTs are stimulated by the appropriate and complex voltage pulses for short-term potentiation (STP) and long-term potentiation (LTP).[28] The regular renewal of synaptic weight is the foundation of procedures for learning and memory, and the weight change is correlated with a presynaptic signal from the neurotransmitter.[29] In a synaptic EGT, the channel conductance (G) represents the synaptic weight (W), and the conductance is also directly related to EPSC. To analyze the STP and LTP modes of the EGTs deeply, a series of voltage pulses (4, 5, and 6 V) with a duration of 40ms are applied to the gate terminal (**Figure 3**a). The peaks of EPSCs are observed to escalate maximums (2.3 mA, 2.2 mA, and 1.1 mA), subsequently slowly decay to the stable value (380, 350, and 65 μA), respectively. Large values of EPSC indicate that ion migration has a significant effect on conductance. Considering that continuous spike input deepens synapse plasticity to be facilitated, a standard principle is proposed that maintains a 3-minute interval between every two tests to ensure the accuracy.[32] Meanwhile, the solution EGTs (AlO_x/InO_x) without Li doping has no STP-LTP response (**Figure S7**). This phenomenon further proves that Li^+ ion plays an irreplaceable role in channel conductance update for neuromorphic computing. Active integration of information is induced from the formation of the STP/LTP in synaptic EGTs, and memory reliability depends not only on the intensity (voltage amplitude) but also on the length (voltage width) of the information.[21] Therefore, the conversion from STP to LTP is similarly realized by increasing the presynaptic pulse width (Figure 3b). This figure indicates that the intensity of EPSCs rise linearly from 50 ms to 400 ms. These peak values (2.5, 2.4, 2.05, 1.7, and 1.1 mA) descend gradually to the stable value (481, 475, 302, 254, and 52 μA), which is also attributed to Li ions accumulate at the AlO_x/InO_x interface. Stimulated by different presynaptic pulse amplitudes and pulse widths, EGTs can realize multi-level storage for neural networks (Figure 3c). The figure also demonstrates the stability of long-term potentiation after 10 minutes and 30 minutes. The characteristic of maintain conductance for a long time further illustrates the excellent synaptic plasticity of EGT. Further, the differences between the initial conductance and the maintained conductance

(refers to error) after 300 minutes are summarized to show the excellent level of stability due to the substantial part of errors below the 0.5% (**Figure S8**). Conductance is positively correlated with the EPSC curve that has the potential for process controlling and parallel computing. Meanwhile, enough large difference between the maximum and minimum conductance (G_{max}, G_{min}) satisfies the neural calculation requirements. Moreover, the gate terminal is then stimulated by a variety of continuous spikes to achieve complex synaptic plasticity. The nonvolatile portion of conductance gradually increased to the saturation state with increasing the pulse number (5, 10, and 15) to demonstrate the effect of continuous multi-pulse on synaptic weight (Figure 3d, e). The transition from STP to LTP occurs as pre-terminal pulses increase from 5 to 15 mainly due to electrochemical doping effects.[22] The initial conductance values increased from the 118μA and finally stabilize at 120 μA (5 pulses), 370 μA (10 pulses), and 490 μA (15 pulses) in 0.8 s, respectively. The three parameters of the Farazdaghi Harris function vary with the frequency and number of pulses (Figure 3h). All fast natural forgetting processes from STP to LTP are accurately fitted by the above function. Moreover, synaptic EGTs exhibit filter characteristics under different series frequencies (1, 2, 5 Hz) of presynaptic pulse signals (Figure 3 f, g). With the series of pulses increases to 5 Hz, the solution-processed synaptic EGTs are applied to verify high-pass filtering characteristics.[34] The potentiation of channel conductance from 180 μA to 620 μA with the frequency increasing from 1 to 5 Hz which can be observed in the case of the initial state value is 100 μA before stimulation. The EGTs with STP/LTP characteristic have limited transmitter release probability which are similar to the biological synapse, and the signal transduction process in neurons is effectively regulated. Consequently, these results can be confirmed that the signal transduction process in EGTs is effectively controlled and the EGTs acquired various electrical stimulation methods to further modify neural communication. For weight updating process in neuromorphic computing, the parameters for emulating the learning process in ANN are extracted from long-term potentiation and long-term depression curves under the 100 positive pulses (5 V, width= 50 ms and Δt = 30 ms) and 100 negative pulses (-4 V, width = 50 ms and Δt = 30 ms). With alternate positive and negative voltage pulses, the synaptic EGTs have excellent LTP/LTD properties to contribute weights update in ANN, such as 100 level conductance states, G_{max}/G_{min} = 67, appropriate A_p (3.1), A_d (-2.7) (Figure 4b). The continuous combination under different conductance states (G) is defined as assessing the nonlinearity of potentiation and depression.

$$G_p = B\left(1 - e^{\left(-\frac{p}{A_p}\right)}\right) + G_{min} \quad (3)$$

$$G_d = -B\left(1 - e^{\left(\frac{p - P_{max}}{A_p}\right)}\right) + G_{min} \quad (4)$$

$$B = (G_{max} - G_{min}) / \left(1 - e^{\left(\frac{-P_{max}}{A_{p,d}}\right)}\right) \quad (5)$$

G_p is the potentiation conductance, G_d is the depression conductance, P_{max} is the maximum number of pulses, and A is the parameter describing the potential and depression nonlinearity. Besides, two curves about ΔG in the potentiation and depression process, which relate to the number of pulses, are plotted **(Figure S9**). The difference between every two neighboring average conductance values is ΔG. The conductance (G) analysis aims to measure the Signal Noise Ratio (SNR) for synaptic transistors.[8] To match higher learning efficiency in the ANN algorithm, the changing trend of G_{max}/G_{min} and nonlinearity with the increase of pulse number under incremental voltage stimulations (4-6 V) are researched (**Figure S10**). The larger G_{max}/G_{min} creates the larger storage range for weight update (under 4 V spike stimulation). Through the analysis of several cycle-to-cycle curves of LTP/LTD, a cycle-to-cycle error was negligible after 10 cycles, showing the excellent robustness of the proposed EGTs device (Figure 4c). The small error originates from the fact that the doped Li^+ ions fill part of oxygen vacancy in the InO_x layer when applying presynaptic pulse and is beneficial to the stability of repeated updating weight (**Figure S11**).

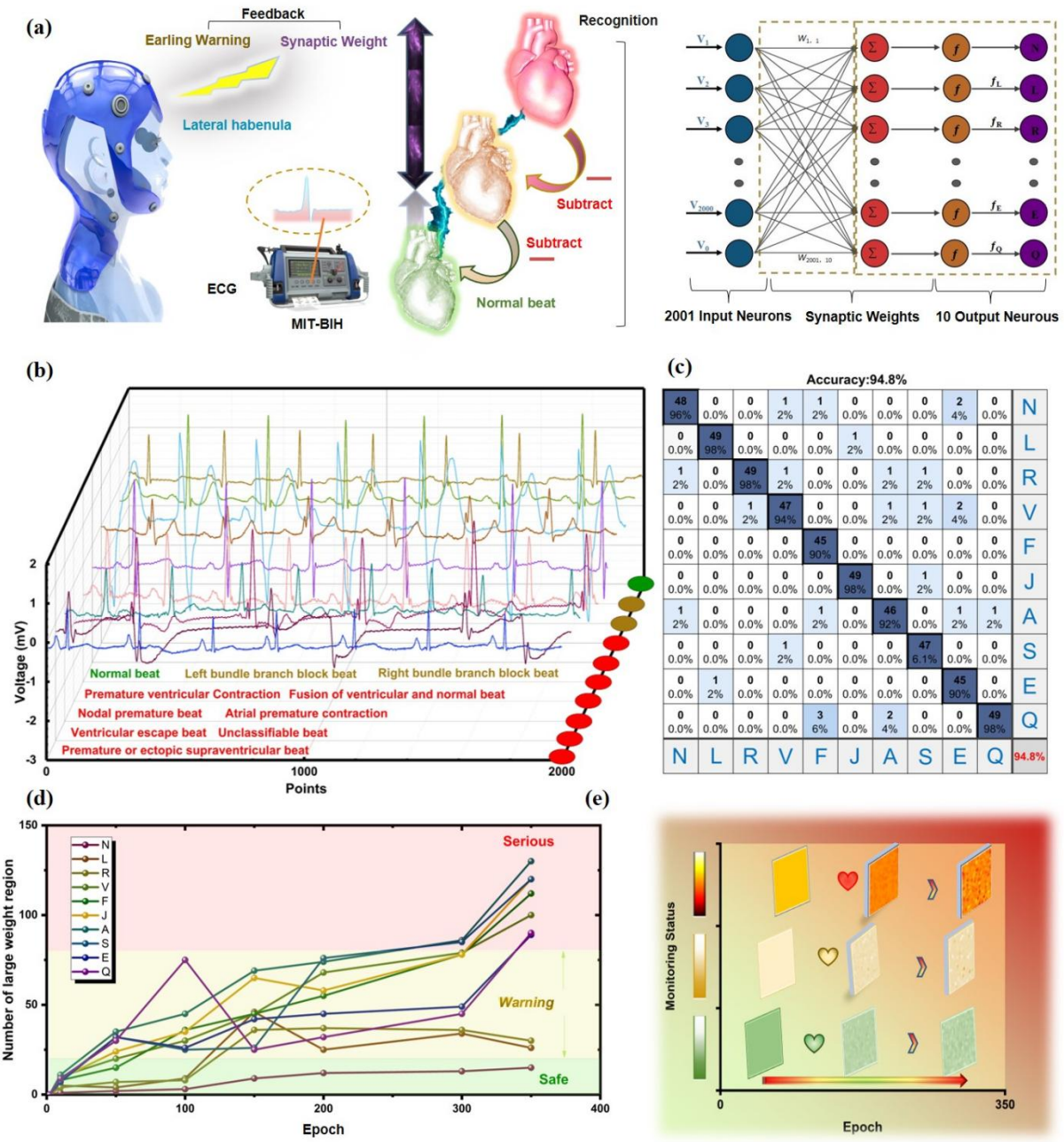

Figure 4. (a) Schematic diagram of cardiovascular abnormality monitoring and timely intervention system. (b) 10 ECG signals from the MIT-BIH database include one normal beat and 9 arrhythmia beats. (c) Confusion map of 10 heartbeat types labeled as N, L, R, V, F, J, A, S, E, Q. (d) Trend of the number of synaptic weight extreme regions in the three states (safe, warning, and serious) with the stimulation time. (e) Synaptic weight map in three monitoring statues with the increase of training epochs.

To further investigate the efficiency and application of the ANN in the field of cardiovascular recognition, we utilized the simulator for training and recognizing ECG signals from the Massachusetts Institute of Technology-Beth Israel Hospital (MIT-BIH) database and extracted

the synaptic weight with multi-level memory for the timely intervention of abnormal heartbeat (Figure 4a).[31] One significance of ECG recognition is related to health care since the abnormal beating of the cardiovascular system cannot be consciously sensed by the brain nerve in time.[36] Recent researches have proven that the specific parts of the brain (Lateral Habenula, LHb) could regulate the cardiovascular system.[27, 28] Therefore, it is possible to intervene and stimulate the LHb to adjust the abnormal heartbeat when a serious heartbeat is recognized. This intervening also due to the number of extreme weight regions exceed a safe and warning threshold. Further, we simulate a single-layer-perception (SLP)-based ANN with the back-propagation algorithm and Manhattan update rules in MATLAB. The training datasets are collected from the Massachusetts Institute of Technology-Beth Israel Hospital (MIT-BIH). The inputs of SLP-based ANN consist of 2001 presynaptic electrical signals, which include 1 bias signal and 2000 input signals. The 2000 input neurons based on time-domain signals of ECG, and 10 output neurons recognize 10 kinds of ECG. In the ANN simulator, the EGTs array is served as a weight unit of iterative operation and is updated due to the error gradient between the weighted sum and expected output. The 10 kinds of ECG signals from the MIT-BIH database include one normal beat and 9 arrhythmia beats, which could be labeled as N, L, R, V, F, J, A, S, E, Q (Figure 4b). According to the extent of the irregularity, these time-domain signals could be divided into three types (safe, warning, and serious) and converted to the input (within 2000 points) of the neural network. The confusion map shows that the 500 ECG matrixes are utilized for the testing section, and the recognition rate achieved 94.8% after 350 epochs (Figure 4c). The more stable and equilibrium recognition rate illustrates that the ECG signal is more suitable for neural networks than MNIST. When the data cannot pass through the neural network at one time, it is necessary to divide the data set into several batches. The **Figure S12** demonstrate the fast operation speed when the more batches (50, 200, 500) added in to the train process of ANN. Besides neural computing, the synaptic weight matrixes based on EGTs as a full connection for error back-propagation also have memory capacity. Moreover**,** The algorithm in ANN need a tradeoff between computing speed and accuracy because One of the drawbacks of electrolyte gate transistor (memory) is conductance decay. To decrease the error caused by the large decay, we adjust update method in algorithm to compensate for the decay during the computing (**Figure S13**). We reconstruct a weight update rule with compensation measures in algorithm according to the recognition rate for different weigh updates frequency (0.1 s, 0.3 s, 0.5 s and 1.0 s) **(Figure S14**). When the computing speed is 0.1 s, the accuracy difference between the test and train process is the 9.5%. The stored weight values of the matrix were extracted from

the training process, showing that the more abnormal beats, the more extreme weight regions (Figure 4d, e). As the number of training epochs is increased to 350, the three areas of safe, warning, and serious were clearly separated. This clearly distinguished result indicates that the network can be designed for Computer-aided Diagnosis and timely intervention systems. This can be expected that in special risk situations without first aid measures, the health management system based on synaptic EGTs can stimulate LHb to enhance heart function when the extreme weight regions beyond the safe threshold.

3. Conclusion

In conclusion, this work demonstrates the practicability of the solution-processed oxide synaptic thin-film transistors. We have proposed an advanced weight update mechanism by voltage spike stimulation that the Li^+ ions accumulate and across between the AlO_x-Li and InO_x-Li layer. EPSC, IPSC, and PPF are basic information flow and the typical manifestation of short-range synaptic plasticity. In this work, we analyze the conductance and nonlinearity that significantly impact the learning accuracy rate based on the LTP/LTD characteristic. Besides simulating the matrix data recognition, the artificial neural network composed of crossbar EGTs array and back-propagation is then developed. Integrated memory and computing synaptic EGTs are utilized as the cardiovascular management system. The Li-doped solution-processed EGTs enriched a variety of synaptic devices alternatives and further evolved in the generation of neural morphological systems as a core component for an intelligent computational machine.

4. Experimental Section

Synthesis of EGTs: The AlO_x precursor solution was obtained by dissolving 2.5M aluminum nitrate hydrate ($Al(NO_3)_3{\cdot}xH_2O$) in 5 ml 2-methoxy ethanol (2-Me). AlO_x-Li precursor solution was obtained by mixing 2.5 M aluminum nitrate hydrate ($Al(NO_3)_3{\cdot}xH_2O$) and 0.25 M indium nitrate hydrate with 10 ml deionized water. The InO_x precursor solution was obtained by dissolving indium nitrate hydrate ($In(NO_3)_3{\cdot}xH_2O$) into 20 mL deionized water. The InO_x-Li precursor solution was obtained by mixing 0.15 M indium nitrate hydrate ($In(NO_3)_3{\cdot}xH_2O$) and 0.015 M LiOH with 20 ml deionized water. All solutions were vigorously stirred under atmospheric conditions for 5 hours and filtered before spin coating using 0.25 μm polytetrafluoroethylene (PTFE) syringe filters, respectively.

Fabrication of Synaptic EGTs:

First, a heavily doped Si (n^{++}) substrate was cleaned by deionized water and dried under N_2 flow. Afterward, the processed substrate was further treated by Plasma for 15 minutes to allow the film surface hydrophilic treatment. The AlO_x and AlO_x-Li films were spin-cast with precursor solution at 3500 rpm for 20 s and then annealed for 30 mins at 200°C in the air atmosphere. The InO_x and InO_x-Li films were spin-cast with precursor solution at 3500 rpm for 30 s and then annealed for 1h at 200°C for the in the air atmosphere. The 30 nm thick Al source/drain(S/D) electrodes were fabricated by thermal evaporation through the shadow mask.

Characterization:

A semiconductor parameter analyzer (Agilent B1500) with transistor characterization software under atmospheric conditions was operated to test the electrical properties of the Li doing InO_x/AlO_x synaptic EGTs. In order to measure the EPSC/ IPSC current flowing between the S/D electrodes, the 0.1 V steady voltage bias was applied to the postsynaptic terminal (V_{post}).[37] Two sets of continuous weight control pulses (Voltage = ±4 V, width = 40ms Δt = 150ms) were added to the weight control terminal to describe each weight state. The surface roughness of the AlO_x, InO_x, AlO_x-Li, and InO_x-Li thin-films were analyzed by atomic force microscopy (AFM). The chemical compositions of dielectric and semiconductor layers were measured by X-ray photoelectric spectroscopy (XPS).

ANNs Simulation:

The calculated conductance of synaptic EGTs in the crossbar array was applied with the positive synaptic weight value. The measurement of the neurocomputing in ANNs includes negative values.[38-40] Subsequently, the synaptic weight ($W = G^+ – G^-$) was expressed as the difference between the state of two synaptic devices (expressed as G^+ and G^-) between each conductance value. The 2001 input neurons corresponded to the 2000 sampling points of ECG and 1 bias input, and the 10 output neurons referred to 10 classes of timing signal. The initial weights were set up random fluctuation near 0 and the value between G_{min} and G_{max} normalized to (-1,1). When the random floating value is less than one learning step in random process, the initial weight will not affect the recognition rate (**Figure S15**).The synaptic weight matrix in the iterative process makes the actual mapping relationship between output (f_{output}-activation function) and input consistent with the expected (f_{expect}) mapping relationship. Actual changed value of weight updating depends on the difference between the conductance state of two synaptic EGTs (G^+ and G^-) which extracted from the LTP/LTD curve. The synaptic weight defined as the difference of conductance in two synaptic EGT which

represent single neuron. When sgn(ΔW) > 0, the formula W ↑= G^+ ↑-G^- ↓ will be used. And when sgn(ΔW) < 0, the W ↓= G^+ ↓-G^- ↑ will be used.

Supporting Information

Supporting Information is available from the Wiley Online Library or the author.

Acknowledgements

This research was funded in part by the Natural Science Foundation of the Jiangsu Higher Education Institutions of China Program (19KJB510059), Natural Science Foundation of Jiangsu Province of China (BK20180242), the Suzhou Science and Technology Development Planning Project: Key Industrial Technology Innovation (SYG201924), University Research Development Fund (RDF-17-01-13), and the Key Program Special Fund in XJTLU (KSF-P-02, KSF-T-03, KSF-A-04, KSF-A-05, KSF-A-07, KSF-A-18).

Received: ((will be filled in by the editorial staff))
Revised: ((will be filled in by the editorial staff))
Published online: ((will be filled in by the editorial staff))

References

[1] J. Sun, S. Oh, Y. Choi, S. Seo, M. J. Oh, M. Lee, W. B. Lee, P. J. Yoo, J. H. Cho, J.-H. Park, *Adv. Funct. Mater.* **2018**, 28, 1804397.

[2] R. Yu, E. Li, X. Wu, Y. Yan, W. He, L. He, J. Chen, H. Chen, T. Guo, *ACS Appl. Mater. Interfaces* **2020**, 12, 15446.

[3] L. Yin, C. Han, Q. Zhang, Z. Ni, S. Zhao, K. Wang, D. Li, M. Xu, H. Wu, X. Pi, D. Yang, *Nano Energy* **2019**, 63, 103859.

[4] C. S. Yang, D. S. Shang, N. Liu, E. J. Fuller, S. Agrawal, A. A. Talin, Y. Q. Li, B. G. Shen, Y. Sun, *Adv. Funct. Mater.* 2018, 28, 1804170.

[5] S. Dai, Y. Zhao, Y. Wang, J. Zhang, L. Fang, S. Jin, Y. Shao, J. Huang, *Adv. Funct. Mater.* **2019**, 29, 1903700.

[6] G. Zhang, Y.-J. Lee, P. Gautam, C.-C. Lin, C.-L. Liu, J. M. W. Chan, *J. Mater. Chem. C* **2019**, 7, 7865.

[7] L. Van Tho, K. J. Baeg, Y. Y. Noh, *Nano Convergence* **2016**, 3, 10.

[8] H. Zhang, Y. Zhang, Y. Yu, X. Song, H. Zhang, M. Cao, Y. Che, H. Dai, J. Yang, J. Yao, *ACS Photonics* **2017**, 4, 2220.

[9] R. C. Naber, K. Asadi, P. W. Blom, D. M. de Leeuw, B. de Boer, *Adv. Mater*. **2010**, 22, 933.

[10] K. J. Baeg, D. Khim, J. Kim, B. D. Yang, M. Kang, S. W. Jung, I. K. You, D. Y. Kim, Y. Y. Noh, *Adv. Funct. Mater*. **2012,** 22, 2915.

[11] X. Ren, *Nat. Mater*. **2004**, 3, 91.

[12] M. F. Tsai, J. Jiang, P. W. Shao, Y. H. Lai, J. W. Chen, S. Z. Ho, Y. C. Chen, D. P. Tsai, Y. H. Chu, *ACS Appl. Mater. Interfaces* **2019**, 11, 25882.

[13] Y. Ni, Y. Wang, W. Xu, *Small* **2021**, 17, 1905332.

[14] S. M. Kwon, S. W. Cho, M. Kim, J. S. Heo, Y. H. Kim, S. K. Park, *Adv. Mater.* **2019**, 31, 1906433.

[15] F. Shan, A. Liu, H. Zhu, W. Kong, J. Liu, B. Shin, E. Fortunato, R. Martins, G. Liu, *J. Mater. Chem. C* **2016**, 4, 9438.

[16] R. Branquinho, D. Salgueiro, L. Santos, P. Barquinha, L. Pereira, R. Martins, E. Fortunato, *ACS Appl Mater Interfaces* **2014**, 6, 19592.

[17] D. Kuzum, R. G. Jeyasingh, B. Lee, H. S. Wong, *Nano Lett* **2012**, 12, 2179.

[18] S. Gao, G. Liu, H. Yang, C. Hu, Q. Chen, G. Gong, W. Xue, X. Yi, J. Shang, R. W. Li, *ACS Nano* **2019**, 13, 2634.

[19] L. Q. Guo, H. Han, L. Q. Zhu, Y. B. Guo, F. Yu, Z. Y. Ren, H. Xiao, Z. Y. Ge, J. N. Ding, *ACS Appl. Mater. Interfaces* **2019**, 11, 28352.

[20 E. K. Jang, Y. Park, J. S. Lee, *Nanoscale* **2019**, 11, 15382.

[21] J. Zhu, Y. Yang, R. Jia, Z. Liang, W. Zhu, Z. U. Rehman, L. Bao, X. Zhang, Y. Cai, L. Song, R. Huang, *Adv. Mater.* **2018**, 30, 1800195.

[22] H. Wei, R. Shi, L. Sun, H. Yu, J. Gong, C. Liu, Z. Xu, Y. Ni, J. Xu, W. Xu, *Nat. Commun.* **2021**, 12, 1068.

[23] J. H. Lim, H.-J. Jeong, K.-T. Oh, D.-H. Kim, J. S. Park, J.-S. Park, *J. Alloy. Compd.* **2018**, 762, 881.

[24] T. Jin, Y. Zheng, J. Gao, Y. Wang, E. Li, H. Chen, X. Pan, M. Lin, W. Chen, *ACS Appl. Mater. Interfaces* **2021**, 13, 10639.

[25] J. Mei, T. Liao, L. Kou, Z. Sun, *Adv. Mater.* **2017**, 29, 1700176.

[26] S. Zhang, K. Guo, H. Han, H. Yu, H. Wei, J. Gong, W. Xu, *Adv. Funct. Mater.* **2021**, 31, 2101917.

[27] T. H. Doan, Y. Sato, M. Matsumoto, T. Koganezawa, *Front. Neurosci.* **2021**, 15, 655617.

[28] Y. Lv, D. Ma, H. Meng, C. Li, W. Lin, *Int. J. Neurosci.* **2012**, 122, 314.

[29] W. He, Y. Fang, H. Yang, X. Wu, L. He, H. Chen, T. Guo, *J. Mater. Chem. C* **2019**, 7, 12523.

[30] I. Sanchez Esqueda, X. Yan, C. Rutherglen, A. Kane, T. Cain, P. Marsh, Q. Liu, K. Galatsis, H. Wang, C. Zhou, *ACS Nano* **2018**, 12, 7352.

[31] J. Li, D. Jiang, Y. Yang, Y. Zhou, Q. Chen, J. Zhang, *Adv. Electron. Mater.* **2020**, 6, 1901363.

[32] J. Kim, Y. Kim, O. Kwon, T. Kim, S. Oh, S. Jin, W. Park, J. D. Kwon, S. W. Hong, C. S. Lee, H. Y. Ryu, S. Hong, J. Kim, T. Y. Heo, B. Cho, *Adv. Electron. Mater.* **2020**, 6, 1901072.

[33] S. K. Kim, Y. Jeong, P. Bidenko, H. R. Lim, Y. R. Jeon, H. Kim, Y. J. Lee, D. M. Geum, J. Han, C. Choi, H. J. Kim, S. Kim, *ACS Appl. Mater. Interfaces* **2020**, 12, 7372.

[34] G. Ding, B. Yang, K. Zhou, C. Zhang, Y. Wang, J. Q. Yang, S. T. Han, Y. Zhai, V. A. L. Roy, Y. Zhou, *Adv. Electron. Mater.* **2019**, 6, 1900978.

[35] M. K. Kim, J. S. Lee, *Nano Lett.* **2019**, 19, 2044.

[36] S. Kim, B. Choi, M. Lim, J. Yoon, J. Lee, H. D. Kim, S. J. Choi, *ACS Nano* **2017**, 11, 2814.

[37] S. Kim, Y. Lee, H.-D. Kim, S.-J. Choi, *Nanoscale* **2020**, 12, 2040.

[38] S. Kim, B. Choi, J. Yoon, Y. Lee, H. D. Kim, M. H. Kang, S. J. Choi, *Sci Rep* **2019**, 9, 11705.

[39] W. He, Y. Fang, H. Yang, X. Wu, L. He, H. Chen, T. Guo, *J. Mater. Chem. C* **2019**, 7, 12523.

[40] Z. Lv, M. Chen, F. Qian, V. A. L. Roy, W. Ye, D. She, Y. Wang, Z. X. Xu, Y. Zhou, S. T. Han, *Adv. Funct. Mater.* **2019**, 29, 1902374.

The neuromorphic computing for the prediction of cardiovascular abnormalities and recognition of matrix data based on eco-friendly synaptic electrolyte gate transistor is proposed to realize the integrated storage and computing function. an artificial neural network (ANN) simulator has been well designed to realize digital image and electrocardiogram (ECG) signal recognition based on the G_{max}/G_{min} and nonlinearity of the EGTs.

Keywords: synaptic transistor, neuromorphic computing, recognition of image and ECG, in-memory computing

Qinan Wang, Tianshi Zhao, Chun Zhao, Wen Liu*, Li Yang, Yina Liu*, Dian Sheng, Rongxuan Xu, Yutong Ge, Xin Tu, Hao Gao, Cezhou Zhao*

Solid State Electrolyte Gate Transistor with Ion Doping for Bio-signal Classification of Neuromorphic Computing.

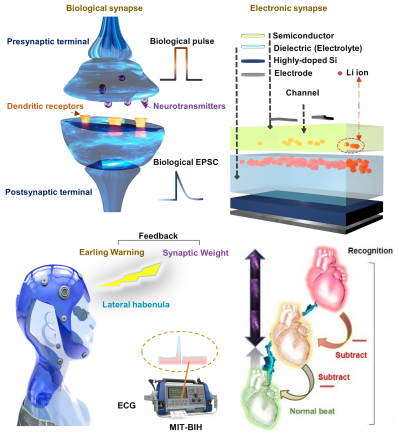

Supporting Information

Visual/Cardiovascular Matrix Information Recognition and Health Warning System based on Synaptic Transistors

Qinan Wang, Tianshi Zhao, Chun Zhao, Wen Liu*, Li Yang, Yina Liu*, Dian Sheng, Rongxuan Xu, Yutong Ge, Xin Tu, Hao Gao, Cezhou Zhao*

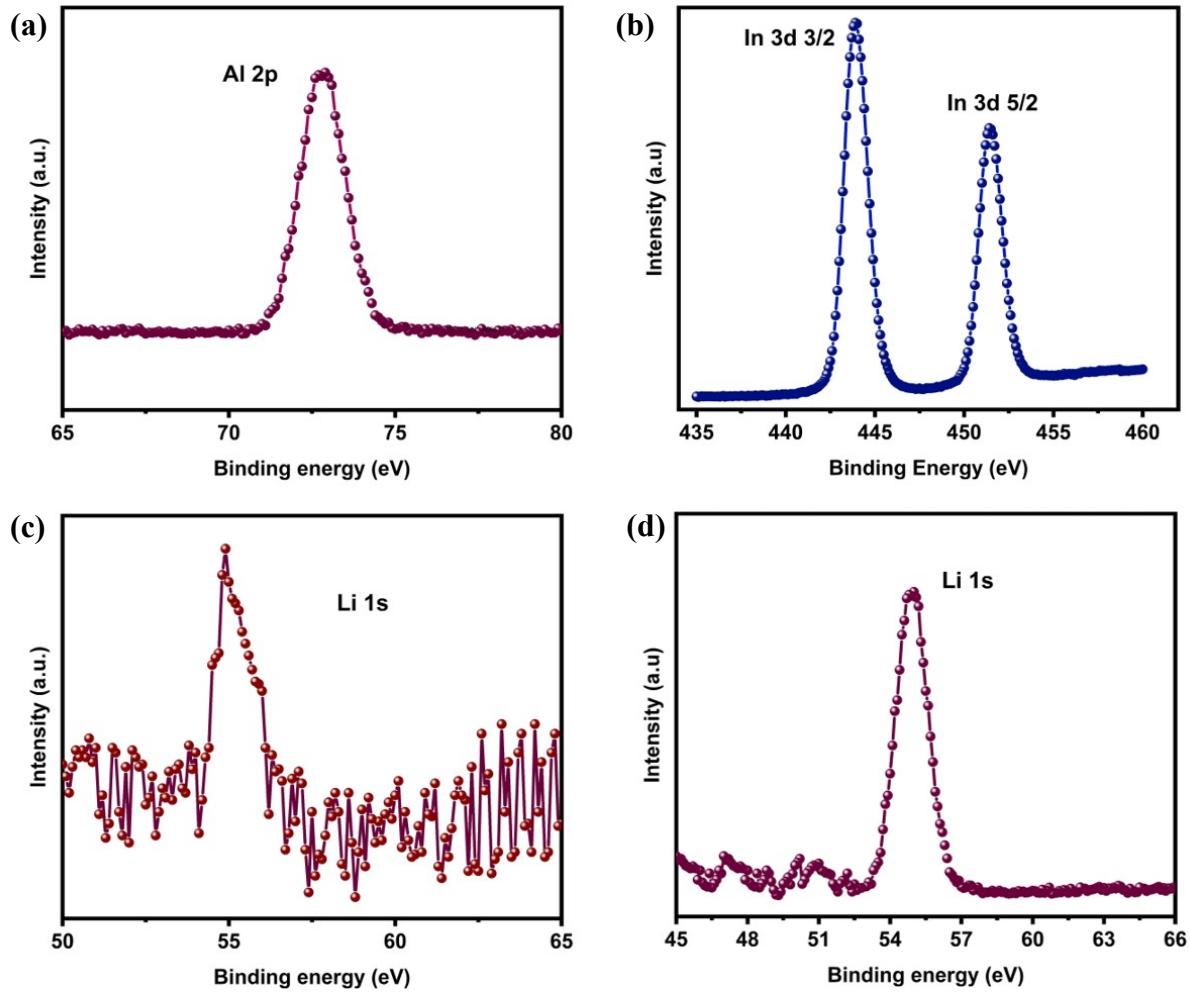

Figure S1. (a) XPS Al 2p spectra for dielectric thin-films. (b) XPS Al In 3d spectra for semiconductor thin-films. (c) XPS Li 1s spectra for dielectric thin-films. (d) XPS Li 1s spectra for semiconductor thin-films.

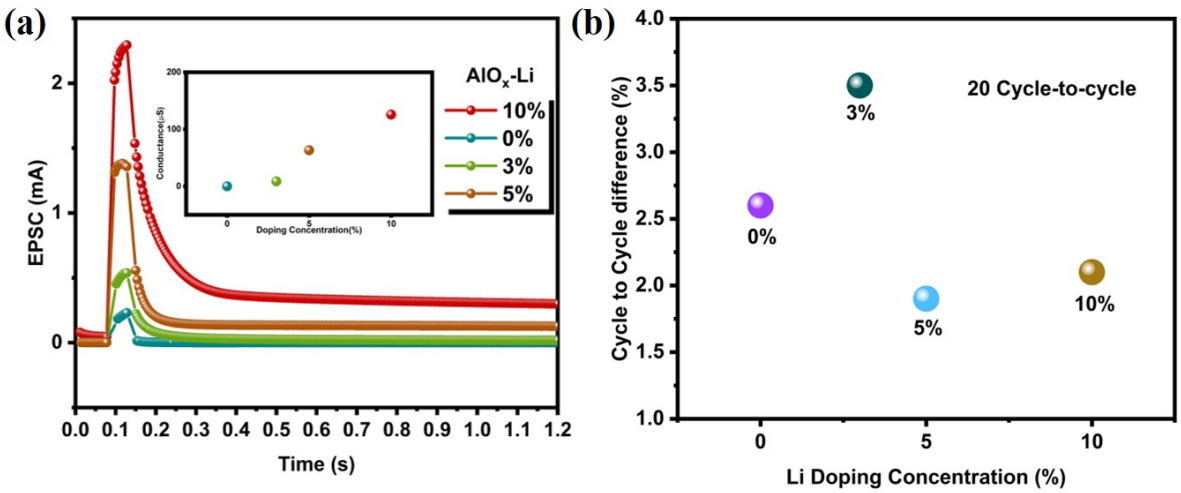

Figure S2. (a) EPSC triggered by spike (6V width=50ms) for different Li doping concentration (0%, 3%, 5%, and 10%) in AlOx thin-films. (b) The cycle-to-cycle difference for different Li doping concentration (0%, 3%, 5%, and 10%) in InOx thin-films.

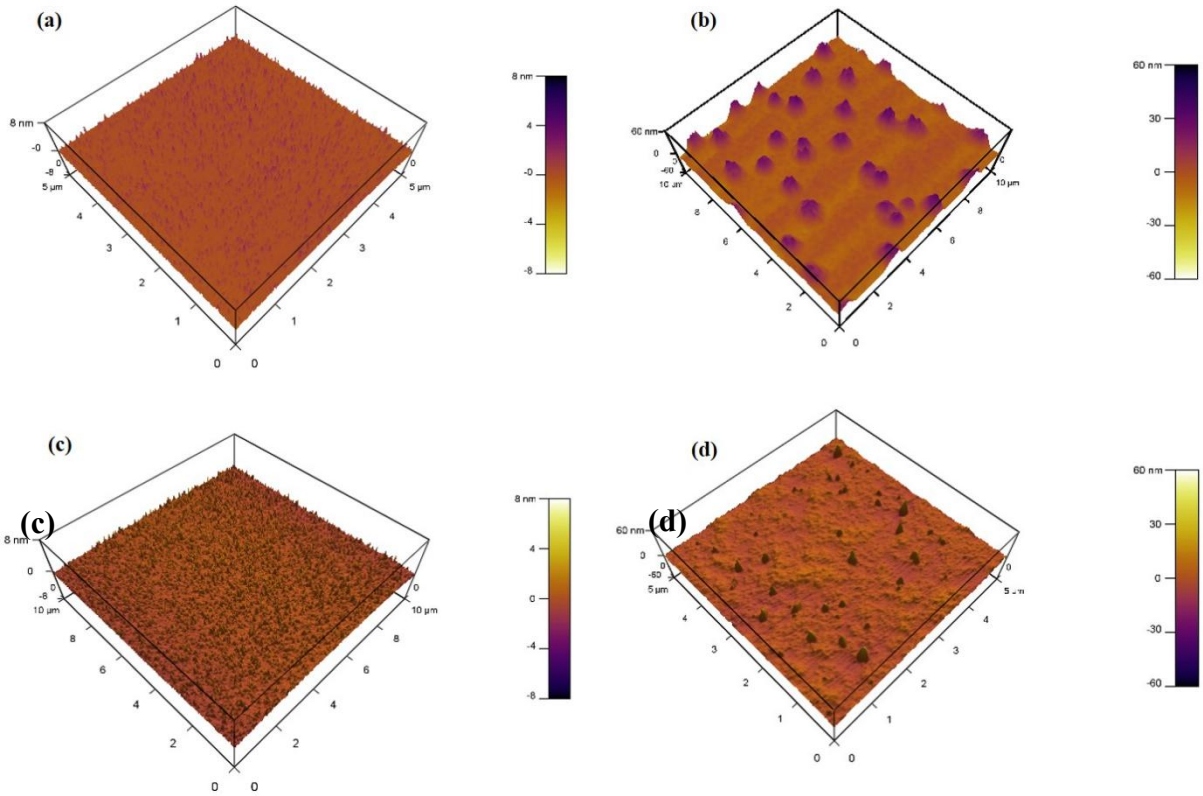

Figure S3. AFM images of (a) AlOx thin-films, (b) AlLiO thin-films, (c) InOx thin-films and (d) InLiO thin-films

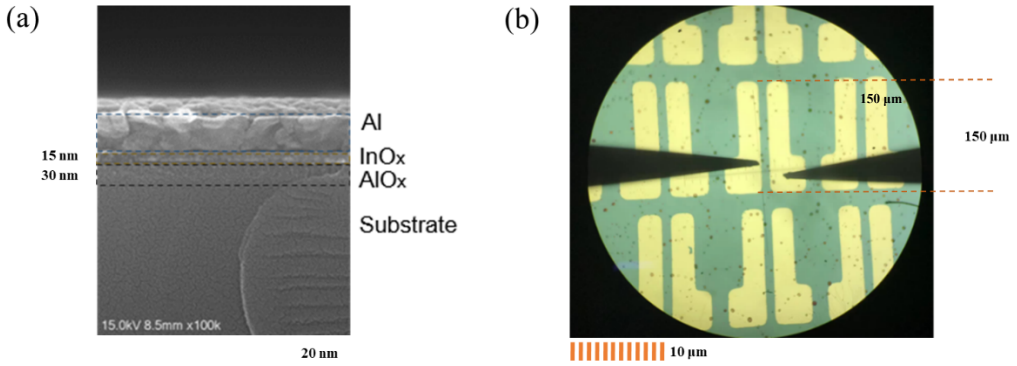

Figure S4. (a) Scanning electron microscope image for the synaptic electrolyte gate transistor. (b) The actual example of the synaptic device (show the drain and source electrodes).

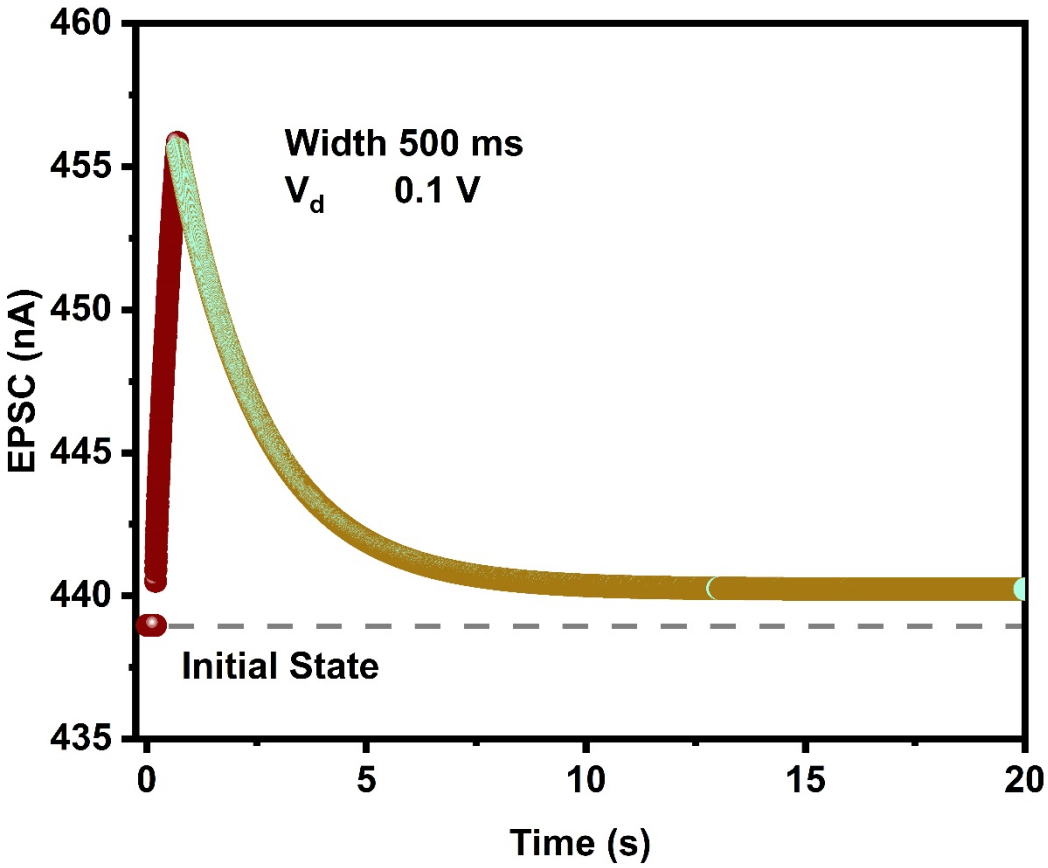

Figure S5. The energy consumption per spike of EGT extracted from the EPSC curve which is triggered by presynaptic spike (V_{gs}=3V, V_{ds}=0.1V, Pulse Width=500ms) in 20 s.

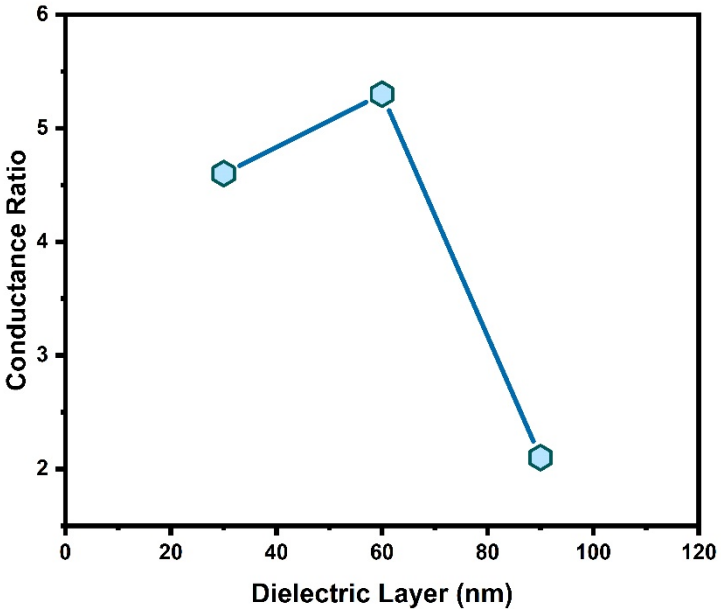

Figure S6. The ratio of stable conductance/ initial conductance for different dielectric layer.

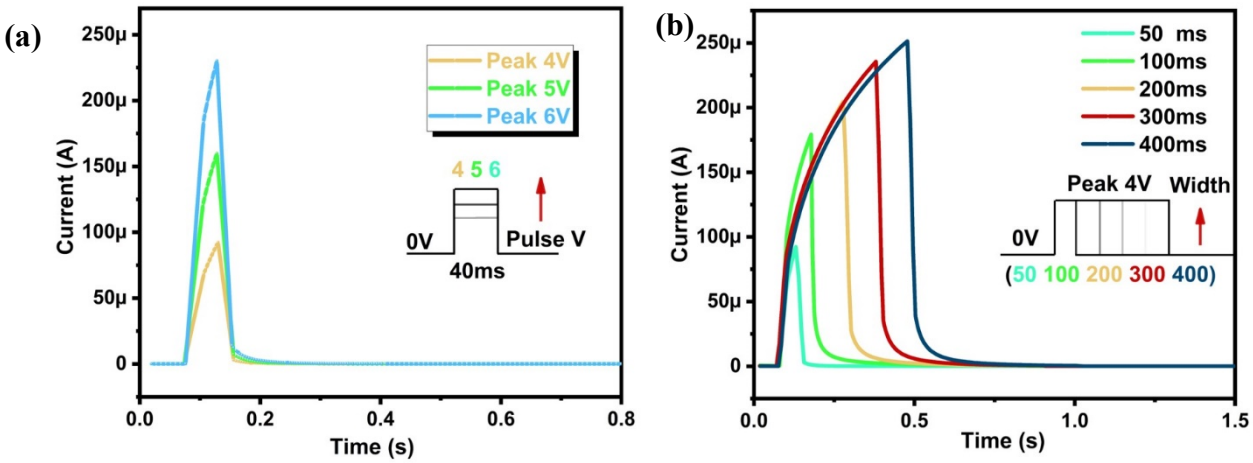

Figure S7. (a) The EPSC triggered by the same width time (40 ms) pulses with three pulse amplitudes (4, 5, and 6 V) at VDS = 4 V without Li ion doped. (b) The EPSC triggered by positive pulses (4 V) with five pulse durations (50, 100, 200, 300, and 400 ms) at VDS=4 V without Li ion doped.

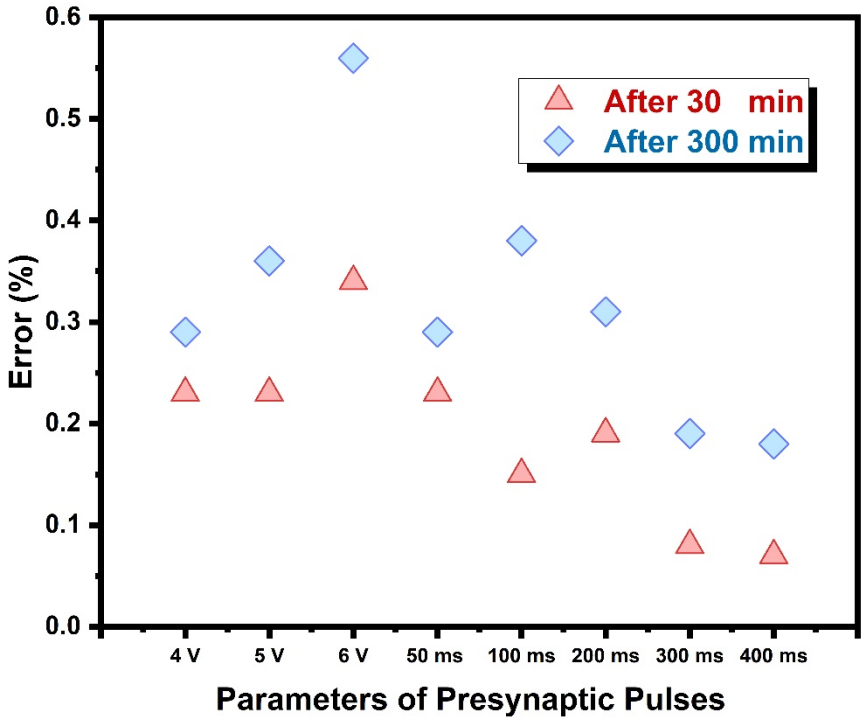

Figure S8. The 30 minutes and 300 minutes error after the presynaptic electric pulse stimulation.

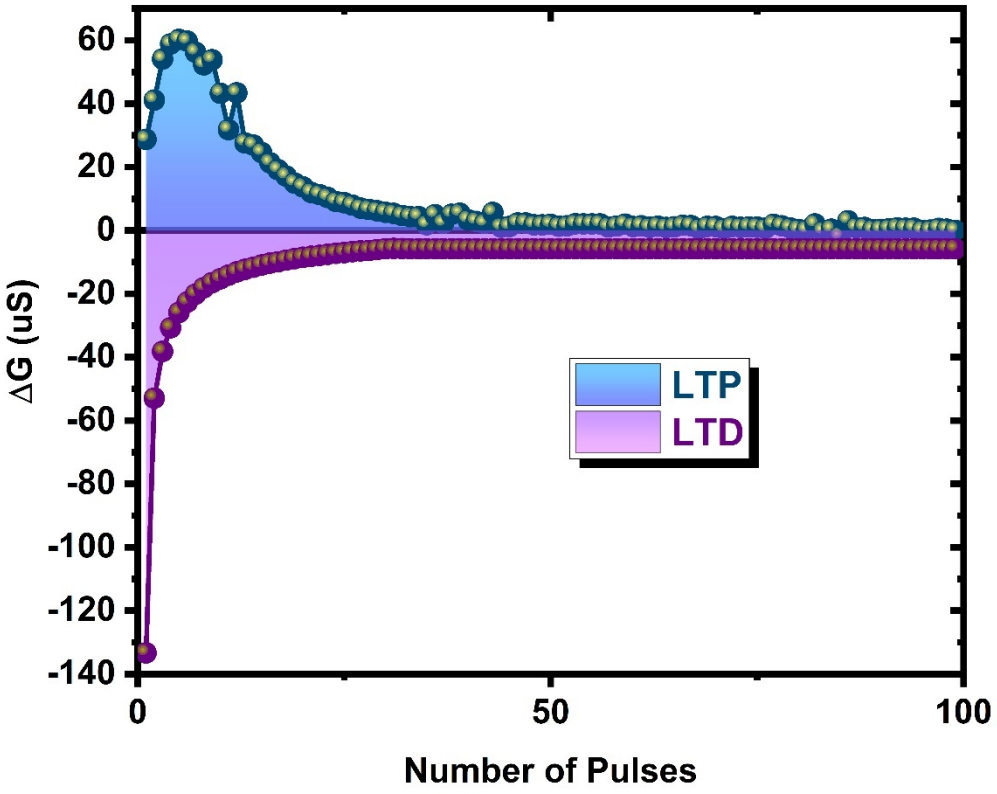

Figure S9. ΔG in the potentiation and depression process

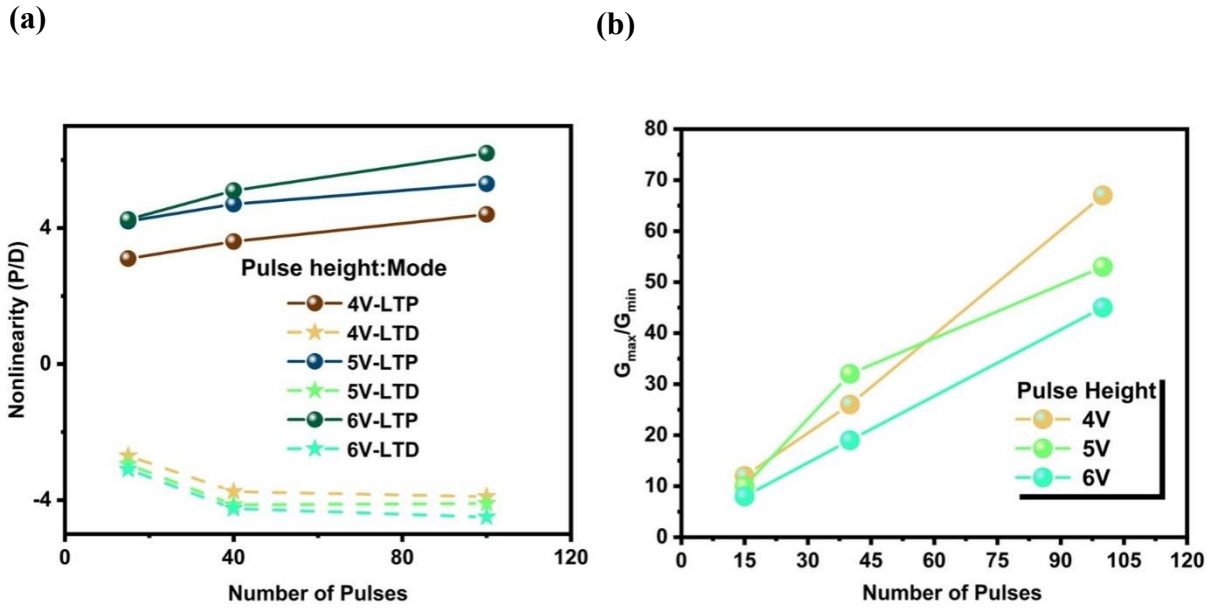

Figure S10. (a) The nonlinearity (NL) change characterized by the LTP/LTD curves with different voltage stimulation (4, 5, and 6 V). (b) G_{max}/G_{min} as functions of (15, 40, and 65) pulses at different pulse heights (4, 5, and 6 V).

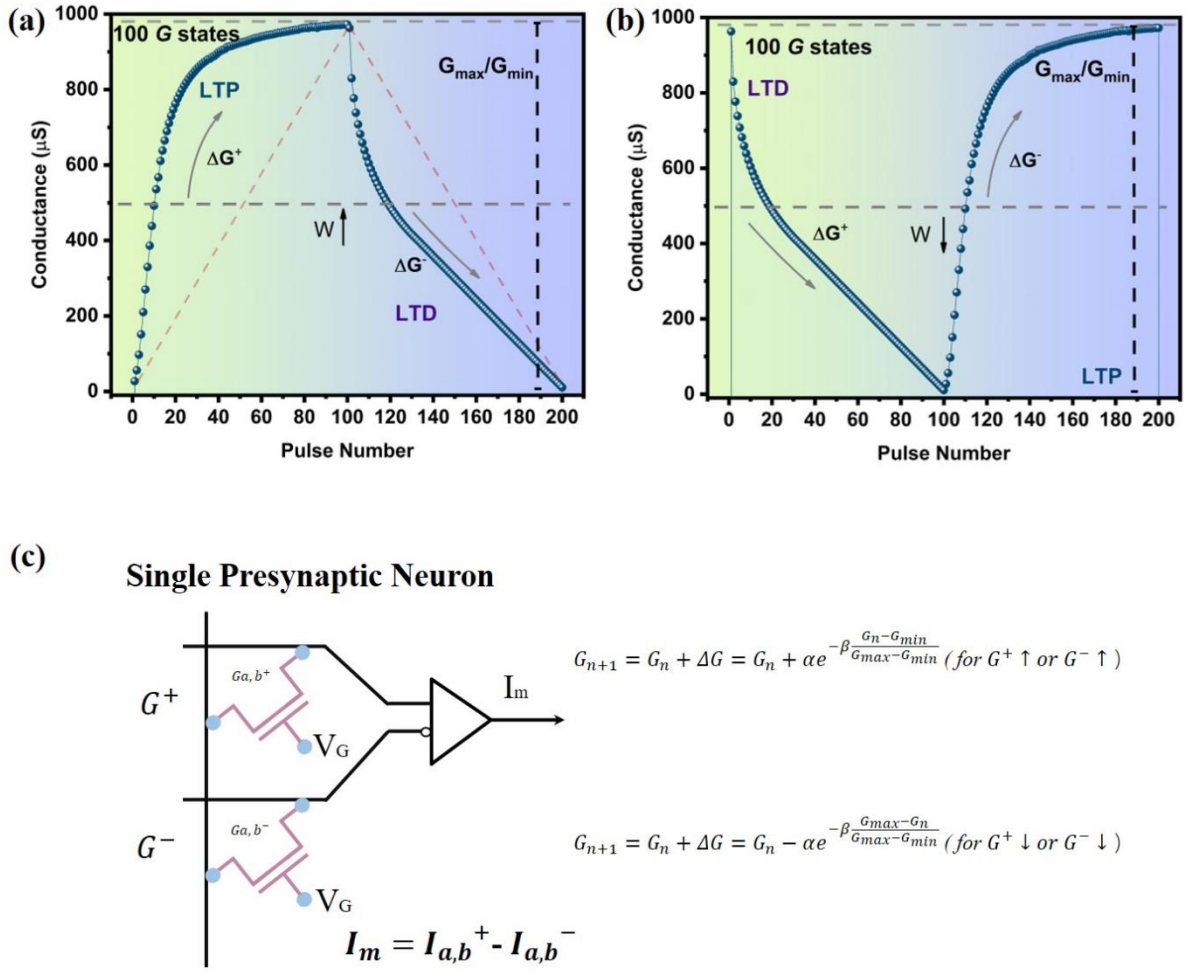

Figure S11. (a) The weight increase method based on the LTP/LTD curve of synaptic EGT. (b) The weight decrease method based on the LTP/LTD curve of synaptic EGT. (c) Two synaptic device represents a signle neural unit in neural network.

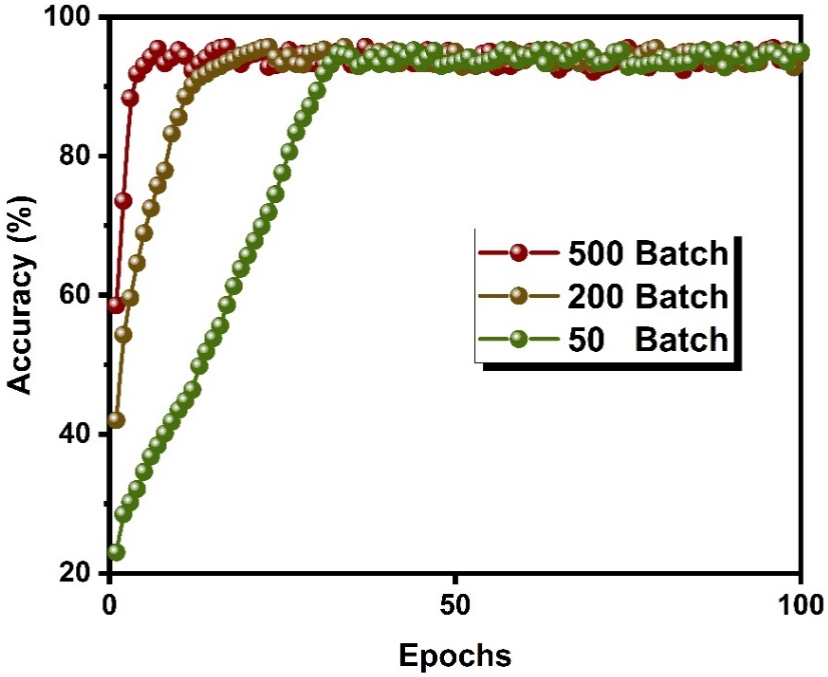

Figure S12. The recognition rate with different batch (500, 200 and 50 batch) for quick speed.

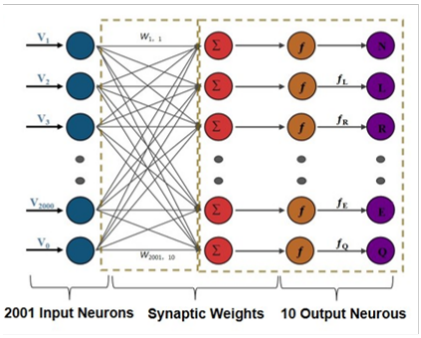

$$\sum = \sum_{j=1}^{2001} W_{jk} V_j \,, \mathrm{k} = 1 - 10 \ (Represent\ 10\ ECG\ signals) = I$$

$$f = \tanh(BI) \ \ (B\ is\ aparameter\ to\ control\ the\ function)$$

Weight update rule

$$W_{jk} = G_{jk}^{+} - G_{jk}^{-} \qquad \Delta W_{jk} = P_{com}\ L_s\ sgn \sum_{n=1}^{2001} \Delta_{jk}(n)$$

$$\Delta_{jk}(n) = \delta_j(n) V_k(n) \qquad \delta_j(n) = [f_e(n) - f_i(n)] \frac{df}{dI}$$

($f_e(n)$ is the expect value, $f_i(n)$ is the output value, L_s is the learning step)

(P_{com} is the compensation parameters for the algorithm)

Figure S13. The algorithm to compensate for the decay during the computing.

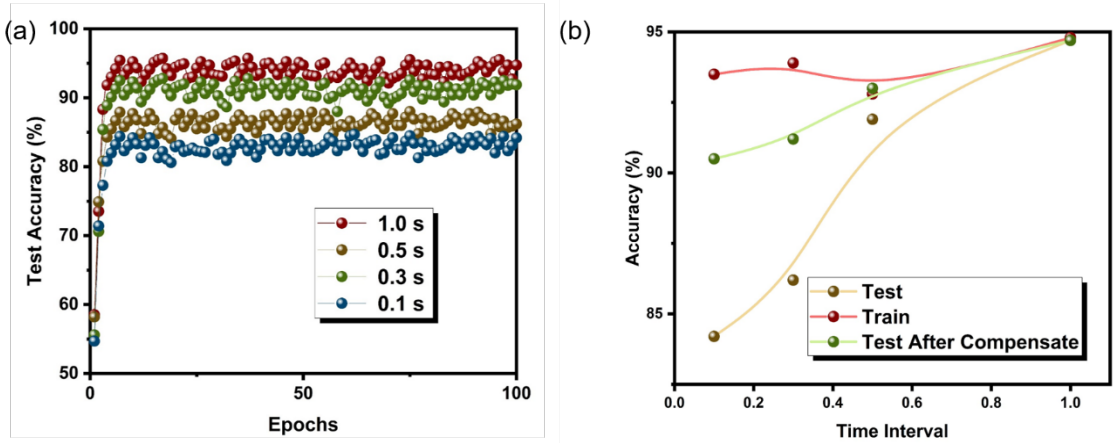

Figure S14. (a) The recognition rate for different weight updates time. (b) The comparison between the different situations (test, train and test after compensate) for recognition rates.

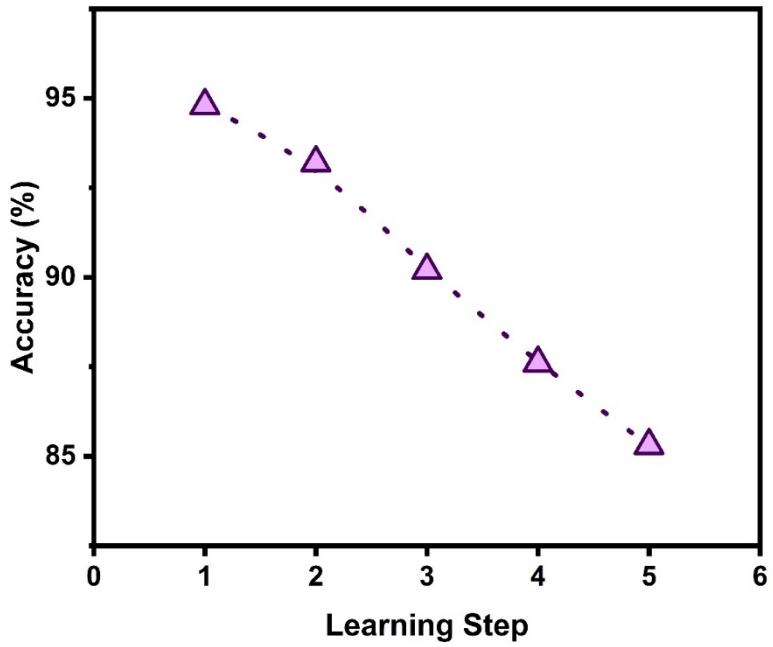

Figure S15. The effect the range of learning step on recognition rate.